CrystEngComm

Cite this: *CrystEngComm*, 2012, **14**, 3163

www.rsc.org/crystengcomm

PAPER

Visible-light-driven photocatalytic and photoelectrochemical properties of porous SnS_x($x = 1,2$) architectures

Junfeng Chao,[a] Zhong Xie,[a] XianBao Duan,[c] Yuan Dong,[a] Zhuoran Wang,[a] Jing Xu,[a] Bo Liang,[a] Bin Shan,[c] Jinhua Ye,[b] Di Chen*[a] and Guozhen Shen*[a]

Received 25th November 2011, Accepted 16th February 2012
DOI: 10.1039/c2ce06586j

By using a facile and template-free polyol refluxing process, we reported the successful synthesis of porous SnS and SnS_2 architectures on a large scale. The as-synthesized samples were characterized by using XRD, SEM, TEM, UV-vis DRS, Raman and N_2 adsorption–desorption analyses. Studies revealed that the as-synthesized SnS and SnS_2 products mainly consist of porous flower-like microstructures with reasonable BET surface areas of 66 $m^2\ g^{-1}$ and 33 $m^2\ g^{-1}$, respectively. Photocatalytic properties of trace amounts of samples were investigated by photodegradation of MB and RhB under visible light irradiation. The photoelectrochemical properties of both samples were also studied by configuring the samples as photoelectrochemical (PEC) cells, exhibiting excellent photosensitivity and response with greatly enhanced $I_{on/off}$ as high as 1.4×10^3, three orders of magnitude higher than previous work. The results indicate the potential applications of the SnS_x nanostructures in visible-light-driven photocatalysts, high response photodetectors and other optoelectronic nanodevices.

Introduction

Porous semiconductor nanomaterials with a large surface area have been widely investigated due to their important applications in many fields such as photocatalysts, optoelectric devices, semiconductor sensors, solar cells and electrode material for batteries and so on.[1–7] Up to now, many synthetic methods have been developed to prepare nanomaterials with porous microstructures. For example, 3D mesoporous carbon structures were successfully fabricated from the soft chemical route using commercially available colloidal silicas as templates.[8] Nanosized flower-like nickel hydroxide, synthesized by a microwave-assisted hydrothermal method, shows good electrochemical activity for the electrochemical reduction of O_2 at room temperature.[9] Hierarchical WO_3 architectures including dendrites, spheres and dumbbells were synthesized from different tungstates with similar morphologies and show enhanced photocatalytic activities for the degradation of some organic dyes compared to the commercial materials.[10] Thus, developing simple and effective methods to fabricate semiconductors with porous structures is important for future device applications.

The photocatalytic technique for the degradation of organic contaminants in solution or in air has attracted extensive interest to remedy the effects of environmental pollution because of its simple and exhaustive decomposition process.[10–14] Among all kinds of semiconductors, TiO_2 is the most investigated one in view of its low cost, good stability, nontoxicity and so on. However, with a wide band gap of 3.2 eV, TiO_2 is only active in the ultraviolet light region and is not responsive to visible light. Although some dyes could be degraded over TiO_2 by self-photosensitization under visible light irradiation, the efficiencies are relatively lower than that under UV light irradiation.[15–18] It is well known that only about 4% of the solar spectra falls in the UV region, thus it is appealing to develop efficient visible light sensitive photocatalysts in view of the better utilization of solar energy. Until now, many researchers have attempted to synthesize new catalysts with narrow band gaps in order to realize visible-light-driven catalytic reactions.[19–25] Metal sulfides have been reported to be promising photocatalysts in the visible region. For instance, ultrathin beta-In_2S_3 nanobelts prepared by Qian's group showed enhanced photocatalytic activity for the decomposition of methyl orange under visible light irradiation.[26] From a two-step solution route, K. Domen and his coauthors have synthesized nanostructured CdS with a high photoactivity for hydrogen evolution when irradiated by visible light.[27]

With narrow band gaps, tin sulfides, one of the IV–VI group semiconductors, include a variety of phases such as SnS, SnS_2, Sn_2S_3, Sn_3S_4 and Sn_4S_5. Among them, SnS and SnS_2, with

[a]*Wuhan National Laboratory for Optoelectronics (WNLO) and College of Optoelectronic Science and Engineering, Huazhong University of Science and Technology (HUST), Wuhan, 430074, China. E-mail: gzshen@mail.hust.edu.cn; dichen@mail.hust.edu.cn; Fax: +86-27-87792225*
[b]*International Center for Materials Nanoarchitectonics (MANA) National Institute for Materials Science (NIMS), 1-2-1 Sengen, Tsukuba, Ibaraki, 305-0047, Japan. E-mail: Jjinhua.YE@nims.go.jp; Fax: (+)81-29-859-2301*
[c]*School of Materials Science and Engineering, Huazhong University of Science and Technology (HUST), Wuhan, 430074, China*

indirect band gaps of 1.3 eV and 2.2 eV, have received more attention due to their possible applications in optoelectronics, solar cells, lithium-ion batteries, near-infrared detectors, photocatalysts and photoluminescence.[28–35] In this paper, we reported the synthesis of porous SnS and SnS_2 architectures from a simple and template-free polyol refluxing route. Photocatalytic properties of both samples were investigated by photodegradation of MB and RhB under visible light irradiation. The electronic structures of the porous SnS and SnS_2 samples were also investigated by band structure calculations. The photoelectrochemical properties of both samples were also studied by configuring the samples as photoelectrochemical (PEC) cells, exhibiting a reasonable photosensitivity and response with greatly enhanced $I_{on/off}$ ratios.

Experimental

Materials

All reagents, such as $SnCl_2 \cdot 2H_2O$, $SnCl_4 \cdot 5H_2O$, thiourea (Tu) and ethylene glycol were analytical grade and used directly without further purification.

Synthesis of SnS and SnS_2 architectures

Porous SnS and SnS_2 architectures were successfully prepared from the simple polygol refluxing process, respectively. In a typical procedure for the SnS sample, appropriate amounts of $SnCl_2$ and Tu were first added into 50 mL ethylene glycol in a round bottom flask. After stirring for 5 min, the reaction system was heated to 175 °C and kept at that temperature for 1 h and then cooled to room temperature naturally. Finally, black precipitates were collected, washed with absolute ethanol and distilled water and then dried at 60 °C. The synthetic process for porous SnS_2 nanostructures was similar to that of SnS products except that $SnCl_4$ was used as the raw material instead of $SnCl_2$ and the refluxing system was kept at 160 °C for 1.5 h.

Material characterization

The crystal structures of the as-prepared samples were confirmed by the X-ray diffraction pattern (X'Pert PRO, PANalytical B.V., the Netherlands) with radiation of a Cu target (Ka, $\lambda = 0.15406$ nm). The morphologies and sizes of the samples were characterized by scanning electron microscopy (SEM, JSM-6700F) and transmission electron microscopy (TEM, JEM-2010). UV-vis diffuse reflectance spectra were recorded on a UV/vis spectrometer (UV-2500, Shimadzu) and were converted from reflection to absorbance by the standard Kubelka–Munk method. The surface areas were measured on a surface area analyzer (Micromeritics, Shimadzu) by nitrogen absorption at 77 K using the Brunauer–Emmett–Teller (BET) method.

Results and discussion

SnS and SnS_2 are two kinds of important layered structured semiconductor materials and the corresponding ball-and-stick models are shown in Fig. 1. Typically, a SnS crystal with orthorhombic structure consists of double layers perpendicular to the *c*-axis in which Sn and S atoms are tightly bound

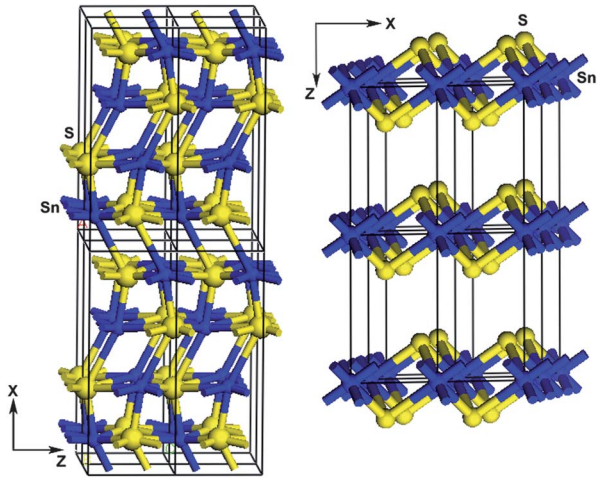

Fig. 1 The ball-and-stick models of SnS (left) and SnS_2 (right) crystals.

(Fig. 1, left). While the SnS_2 with hexagonal cadmium iodide (CdI_2) structure is composed of sheets of tin atoms sandwiched between two close-packed sheets of sulfur atoms (Fig. 1, right). Based on the layered structure properties, research on SnS and SnS_2 has attracted more and more attention.

XRD was used to study the phase purity of the as-synthesized SnS and SnS_2 products as shown in Fig. 2. All of the peaks in the XRD pattern in Fig. 2a can be readily indexed to the pure orthorhombic SnS phase with space group *P6nm* (JCPDS card No: 39-354). The pattern in Fig. 2b can be indexed to the hexagonal SnS_2 phase with space group *P*-3*m*1 (JCPDS card No: 23-677). Clearly, no characteristic peaks from other crystalline impurities were detected in these XRD patterns, indicating the formation of pure products.

Raman spectroscopy is an appropriate technique to probe the detailed structure of materials because the bonding states in the coordination polyhedra of a material can be deduced directly from the Raman vibrational spectrum. In orthorhombic SnS, 24 vibrational modes are represented by the following irreducible representations at the center of Brillouin zone as:

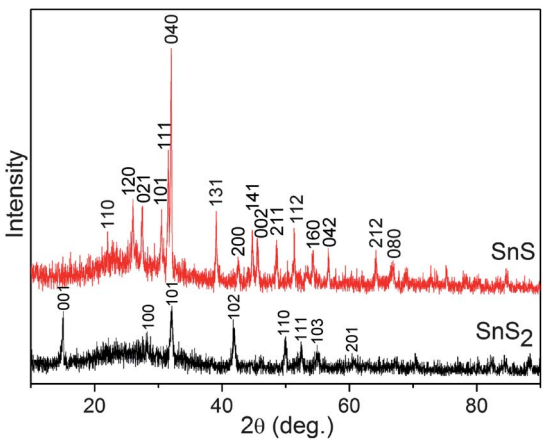

Fig. 2 XRD patterns of the as-synthesized porous SnS and SnS_2 architectures.

$$\Gamma = 4A_g + 2B_{1g} + 4B_{2g} + 2B_{3g} + 2A_u + 4B_{1u} + 2B_{2u} + 4B_{3u}$$

Among them, there are 21 optical phonons, of which 12 are Raman active modes ($4A_g$, $2B_{1g}$, $4B_{2g}$ and $2B_{3g}$), seven are infrared active modes ($3B_{1u}$, $1B_{2u}$ and $3B_{3u}$) and two are inactive ($2A_u$).[36] Fig. 3 shows the Raman spectra of the as-synthesized SnS and SnS_2 products, respectively. The Raman modes shown in Fig. 3a are observed at 69, 95, 165, 192 and 219 cm^{-1}, respectively. Among the peaks, the peaks at 69 cm^{-1}, 95 cm^{-1}, 165 cm^{-1} corresponding to the B_{1g} or B_{2g} mode, A_g mode and B_{3g} mode, respectively, are in good agreement with the literature.[37] The peaks at 192 cm^{-1} and 219 cm^{-1} can be assigned to the A_g mode. The Raman spectrum of the as-synthesized SnS_2 is shown in Fig. 3b. A strong Raman peak located at about 313 cm^{-1} is observed, which can be assigned to the A_{1g} mode according to the group theory analysis given by Lucovsky *et al.*[38] According to the Raman results, it can be further confirmed that pure phase SnS and SnS_2 products were prepared from the present process.

The morphology and microstructure of the as-prepared sulfides from the simple polyol refluxing process were characterized by SEM. Fig. 4a shows the low-magnification SEM image of SnS products, which demonstrates that porous SnS samples on a large scale were prepared and composed of many nanoplatelets with uniform size. Further observation (Fig. 4b) depicts that large numbers of platelets interconnect with each other with a thickness of several tens of nanometres to form a porous architecture structure. In the present case, a similar porous architecture structure was also observed in SnS_2 products as shown in Fig. 4c, when the raw material of $SnCl_4$ was used in this refluxing solution at 165 °C. The high-magnification FESEM image of the products in Fig. 4d indicates that the surfaces of the architectures are highly porous in structure, suggesting that the samples possess possibly large surface areas. The measurements show that the BET surface areas of porous SnS and SnS_2 architectures are 66 $m^2\ g^{-1}$ and 33 $m^2\ g^{-1}$, respectively, which are favourable for potential applications in waste water treatment such as photocatalysts.

Further insight into the microstructural details of the porous SnS and SnS_2 architectures were gained by using TEM and high-resolution TEM (HRTEM). Fig. 5a shows a TEM image taken from the porous SnS architectures. It is interesting that the SnS products are composed of interconnected nanoplatelets, in good accordance with the SEM observations. The representative HRTEM image (Fig. 5b) taken from the edge of the microstructures exhibits the highly crystalline nature of the SnS nanoplatelets. The lattice fringe in the image is clearly visible with a spacing of 0.40 nm, corresponding to the (110) plane of orthorhombic SnS. Fig. 5c displays the TEM image of the SnS_2 product. Nanoplatelets with a thickness of about several nanometres were found to be connected to each other to build the 3D porous architectures. This is also in good agreement with the SEM results. The distance between the lattice fringes of the architectures can be indexed to the (100) planes of hexagonal SnS_2.

The optical properties of the products were measured and the corresponding UV-vis absorption spectra are depicted in Fig. 6a. A black-colored SnS sample (inset in Fig. 6a) exhibits broad and strong absorption in the range from 200 to 800 nm. In contrast, yellow-colored SnS_2 (inset in Fig. 6a) only absorbs light in the region below 600 nm and it exhibits less intensive absorption

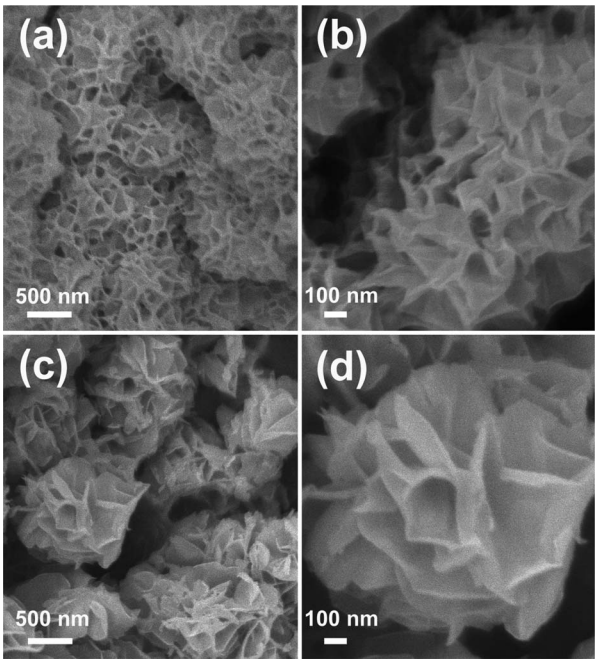

Fig. 4 SEM images of the as-synthesized porous SnS (a, b) and SnS_2 (c, d) architectures from the simply polyol refluxing process.

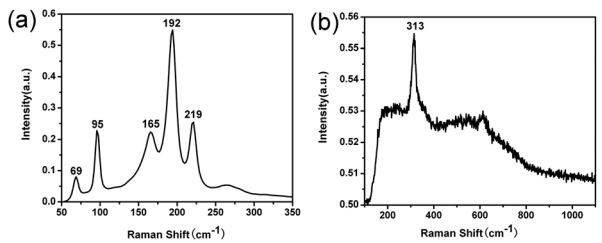

Fig. 3 Raman spectra of the as-synthesized porous SnS (a) and SnS_2 (b) architectures.

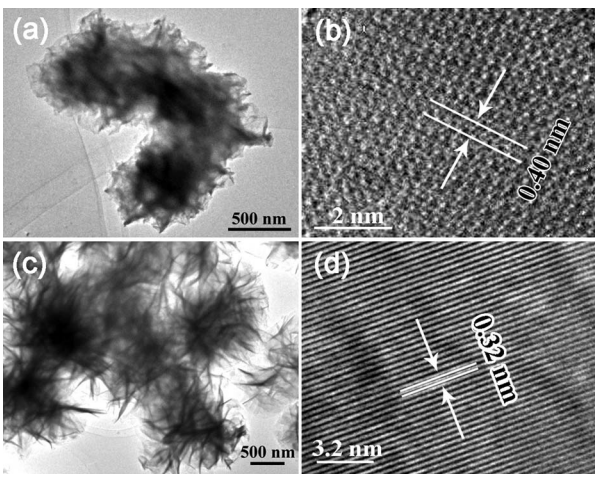

Fig. 5 TEM and HRTEM images of the porous SnS (a, b) and SnS_2 (c, d) architectures from the simple polyol refluxing process.

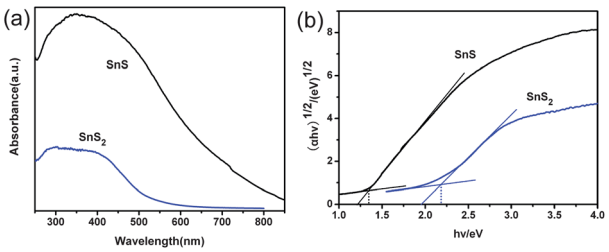

Fig. 6 (a) UV-vis absorption spectra and (b) $(\alpha h\nu)^{1/2}$ *vs.* $h\nu$ plots for the porous SnS and SnS_2 architectures.

compared to the SnS sample. The optical band gaps of the two samples could be evaluated from the following equation:[39–41]

$$\alpha h\nu = A(h\nu - Eg)^{n/2}$$

Here α, ν, A, Eg and n are the absorption coefficient, incident light frequency, constant, optical band gap, and an integer (normally equal to 1, 2, 4 and 6), respectively. The n values for the two observed optical transitions for the two samples should be indirect. The α and ν values at the steep edges of the absorption spectra were used to construct the plots of $(\alpha h\nu)^{2/n}$ against photon energy. As seen in Fig. 6b, the curves for the two samples show a linear region with $n = 4$ for the indirect band gap. The optical band gaps of the samples could be determined by the intersections of the extrapolated linear portions of the plots with the energy axis. These values were calculated to be about 1.35 eV for SnS and 2.18 eV for SnS_2, which is in good agreement with the previous reports.[42,32]

To investigate the photocurrent properties of the as-synthesized SnS and SnS_2 products, photoelectrochemical (PEC) cells were prepared by using the as-synthesized products as the corresponding photoelectrode, respectively. The photoelectrodes of the photoelectrochemical devices were prepared by the well-known "doctor-blading" method widely used for dye-sensitized solar cell (DSSC) fabrication. The corresponding SnS or SnS_2 product was first deposited onto a FTO substrate. The counterelectrode was lightly platinized by coating with a drop of an isopropanol solution of H_2PtCl_6, followed by firing at 400 °C for 20 min. A solar simulator of AM 1.5G (100 mW cm^{-2}) was used as the illumination source. In principle, when the external circuit was closed, the illuminated PEC devices should generate a photocurrent. Fig. 7 demonstrates the typical time-dependent current change curves of the PEC devices made of SnS and SnS_2 architectures, respectively. From Fig. 7a, we can see that, upon illumination, the current density rapidly increased from 0.052 μA cm^{-2} to a stable value of 70.5 μA cm^{-2}. The significant enhancement of the current density induced by electron-hole generation is around 1.4×10^3. Similar results were also obtained for the SnS_2 architectures, as can be seen in Fig. 7b. Both values are about three orders of magnitude higher than previous work on the same materials.[43] Besides, there are current transients in both the light-on state and the light-off state, which can be attributed to a typical sign of surface recombination processes according to previous reports.[44–46]

It was found that the photocurrent response can be reproducibly switched from the "ON" state to the "OFF" state by periodically turning the solar simulator on and off. When

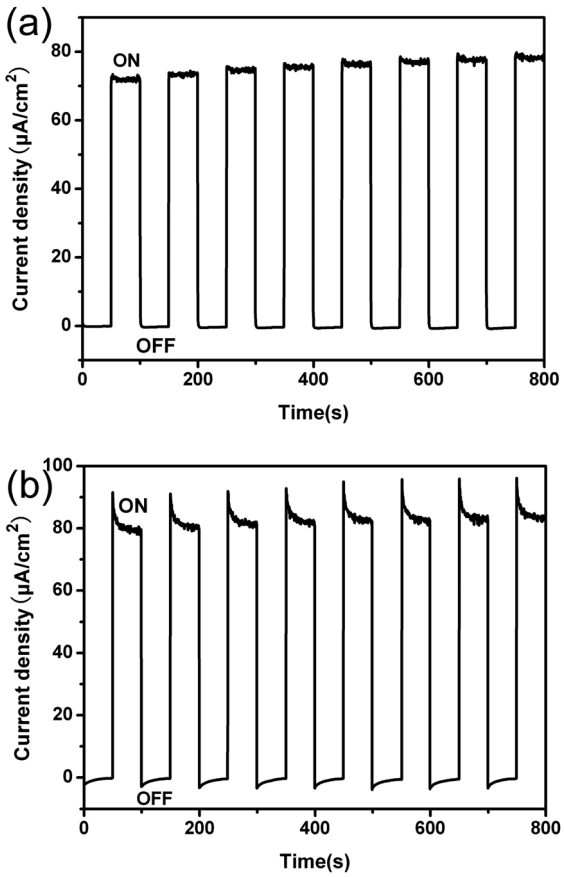

Fig. 7 *J–T* curves of the porous SnS (a) and SnS_2 (b) architectures under one sun illumination (AM 1.5G).

switched from the dark to light condition, the photocurrent response of the SnS-based PEC device changes abruptly and then stably with time (in Fig. 7a), while the response curve of the SnS_2-based PEC device has a sharp-edged peak at first and then drops slowly (in Fig. 7b). The response time and decay time of both devices were around 0.5 s, indicating rapid photoresponse characteristics. On the other hand, the relatively low dark current also guarantees the outstanding optical switch performance for the device. When the solar simulator illuminates, photons with energy higher than the SnS_x band gap are absorbed by the SnS_x nanomaterials and a lot of electron–hole pairs are generated. The holes accept electrons from the I^{3-}/I^- redox electrolyte, and the electrons move from the porous SnS_x surface to the anode contact. Along with the photocurrent flows, electrons pass through the external closed circuit. Owing to the porous surface area, the practical contact area of the device is much larger than the flat light area, so the number of electron–hole pairs created can be tremendously larger than that of the geometric device area.

The photocatalytic activities of the as-synthesized porous SnS and SnS_2 architectures were further evaluated for the degradation of some organic dyes such as methylene blue (MB) and rhodamine B (RhB) under visible light irradiation at room temperature. Since both samples possess large BET surface areas, trace amounts of the SnS (10 mg) and the SnS_2 (20 mg) samples were used in the present cases, respectively. First, an appropriate

catalyst was suspended into 100 mL MB or RhB aqueous solution in a pyrex reactor, respectively (the dye concentration was 8 mg L^{-1} in both cases). The suspension was stirred in the dark for a certain time to reach an adsorption–desorption equilibrium, then the light was turned on. A 500 W Xe-lamp equipped with a cutoff filter ($\lambda > 420$ nm) and a water filter was used as the light source. At given irradiation time intervals, appropriate reaction suspension was collected and filtrated. The absorption spectra of the filtrates were measured on a Shimadzu UV-2550 UV-vis spectrometer and are shown in Fig. 8. Clearly, during the dark, porous SnS architectures with a larger BET surface area of 66 m^2 g^{-1} showed higher adsorption abilities to MB and RhB than the SnS_2 product. As shown in Fig. 8(a–d), porous SnS architectures can adsorb about 75% of MB within 30 min. The dye concentration adsorbed onto the surface of the catalyst further increases with the prolonging of time (Fig. 8b). After 2 h, an adsorption–desorption equilibrium in the solution was reached, since the intensities of the main peaks located in the visible region and in the UV region are similar to those for 2.5 h. When the light was turned on, the main peaks decreased continuously with increased irradiation time, indicating that the MB solution was decomposed completely in the present system. Fig. 8(c,d) shows the great adsorption and degradation activities of the SnS architectures when trace catalyst was dispersed into the RhB solution. Due to the good adsorption and degradation effect of the SnS architectures exhibited in the organic dye solution, we can conclude that the obtained sample might be used in the wastewater treatment in industry.

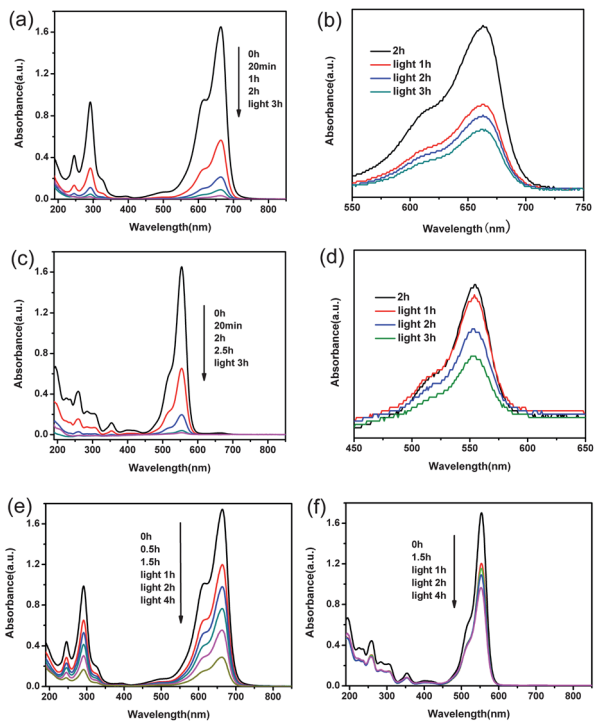

Fig. 8 (a,b) UV-vis spectral changes of MB aqueous solution and the magnification of the lit portion,(c,d) UV-vis spectral changes of RhB aqueous solution and the magnification in the presence of SnS architectures and (e) MB aqueous solution and (f) RhB aqueous solution in the presence of SnS_2 architectures under visible light irradiation. Reaction conditions: 100 mL, 8 mg L^{-1}, 500 W Xe-lamp, $\lambda > 420$ nm.

In addition, the photocatalytic abilities of the porous SnS_2 architectures were also investigated and Fig. 8(e,f) show the photodegradation process of MB and RhB solutions in the presence of SnS_2 catalysts, respectively. It was obvious that the porous SnS_2 products with less BET surface area show weaker adsorption and photocatalytic abilities compared to the porous SnS architectures. However, in our experiments, we found that trace amounts (10 mg or 20 mg) of the two samples can accomplish good adsorption and degradation to the MB and RhB when irradiated by visible light, which is better or comparable to previous reports.[33,47–50]

The photocatalytic performances of sulfide photocatalysts strongly depend on their electronic structures. In the present work, the electronic structures of SnS and SnS_2 were further investigated by plane-wave DFT calculations, respectively, and Fig. 9 shows the energy structures and density of states (DOS) calculated. As shown in Fig. 8a left, the conduction band minimum (CBM) of SnS crystal is located in the area between the G point and the Z point while the valence band maximum (VBM) is located at the Y point of Brillouin zone, indicating that SnS is indeed an indirect semiconductor. Similarly, the calculated energy band of SnS_2 is shown in Fig. 9b left, it can be clearly seen that the conduction band minimum (CBM) of SnS_2 crystal is located at the M point of the Brillouin zone and the valence band maximum (VBM) is located in the region between the K point and the G point, indicating that SnS_2 is also an indirect semiconductor. For an indirect semiconductor, the lifetime of the photoexcited electron–hole pair is comparably longer than that in the direct samples, which is beneficial for the photocatalytic reactions. The band gap of a given semiconductor is determined mainly by the potential of the valence band top and the potential of the

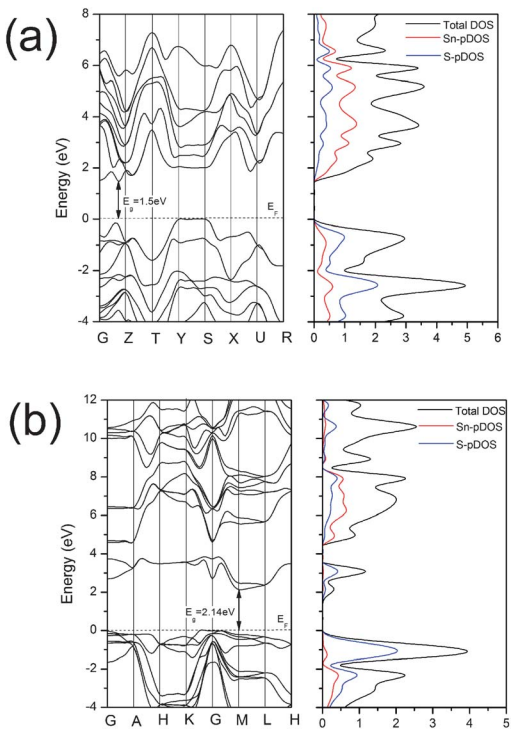

Fig. 9 The calculated (left) energy bands and (right) density of states (DOS) of as-synthesized porous (a) SnS and (b) SnS_2 samples.

conduction band bottom. The total DOS displays (Fig. 9a and 9b right) that the bands of SnS and SnS_2 are classified into two parts. The bottom of the conduction band is mainly constituted by the Sn 5p orbital, while the conduction band top is composed mainly of the S 3p orbital. The band structure indicates that charge transfer upon photoexcitation occurs from the S 3p orbital to the empty Sn 5p orbital. The calculated band gaps of SnS and SnS_2 are 1.5 and 2.14 eV, respectively, which are slightly larger than the experimental results based on the UV-vis absorption spectra.

Conclusions

In summary, we reported the synthesis of porous SnS and SnS_2 architectures from the simple polyol refluxing process on a large scale. SEM investigations revealed that both the SnS and the SnS_2 products are composed of many nanoplatelets interconnecting with each other to form the porous architecture. The photoelectrochemical characteristics recorded under AM 1.5 illumination exhibited the increased photoresponse properties of SnS and SnS_2 based devices. Greatly enhanced $I_{on/off}$ with a value of about 1.4×10^3, three orders of magnitude higher than previous work, was obtained. Furthermore, during the photocatalytic degradation process, black SnS architectures with a larger BET surface area and the narrower band gap of 1.35 eV show much stronger adsorption and photodegradation abilities for MB and RhB solutions compared to yellow SnS_2 products. Our results indicate the potential applications of the SnS_x nanostructures in visible-light-driven photocatalysts, high response photodetectors and other optoelectronic nanodevices.

Acknowledgements

This work was supported by the National Natural Science Foundation (21001046, 51002059), the 973 Program of China (No.2011CB933300, 2011CBA00703), the Basic Scientific Research Funds for Central Colleges (2010QN045), the Research Fund for the Doctoral Program of Higher Education (20090142120059, 20100142120053) and the Director Fund of WNLO. We thank the Analytical and Testing Center of Huazhong University Science & Technology, and the Center of Micro-Fabrication and Characterization (CMFC) of WNLO for the samples measurements.

Notes and references

1 C. McManamon, J. D. Holmes and M. A. Morris, *J. Hazard. Mater.*, 2011, **193**, 120.
2 T. Kokubu, Y. Oaki and E. Hosono, *Adv. Funct. Mater.*, 2011, **21**, 3673.
3 Y. S. Li, J. Xu, J. F. Chao, D. Chen, S. X. Ouyang, J. H. Ye and G. Z. Shen, *J. Mater. Chem.*, 2011, **21**, 12852.
4 K. Varoon, X. Y. Zhang and B. Elyassi, *Science*, 2011, **334**, 6052.
5 Z. X. Yang, G. D. Du, Z. P. Guo, X. B. Yu, Z. X. Chen, T. L. Guo and R. Zeng, *Nanoscale*, 2011, **3**, 4440.
6 Z. X. Y. G. Zhu, J. Xu, H. T. Huang, D. Chen and G. Z. Shen, *CrystEngComm*, 2011, **13**, 6393.
7 T. N. Huan, T. Ganesh, K. S. Kim, S. Kim, S. H. Han and H. Chung, *Biosens. Bioelectron.*, 2011, **27**, 183.
8 H. I. Lee, G. d. Stucky, J. H. Kim, C. Pak, H. Chang and J. M. Kim, *Adv. Mater.*, 2011, **23**, 2357.
9 L. P. Xu, Y. S. Ding, C. H. Chen, L. L. Zhao, C. Rimkus, R. Joesten and S. L. Suib, *Chem. Mater.*, 2008, **20**, 308.
10 D. Chen and J. H. Ye, *Adv. Funct. Mater.*, 2008, **18**, 1922.
11 D. Chen, Z. Liu, S. X. Ouyang and J. H. Ye, *J. Phys. Chem. C*, 2011, **115**, 15778.
12 M. A. Fox and M. T. Dulay, *Chem. Rev.*, 1993, **93**, 341.
13 D. Chen, S. X. Ouyang and J. H. Ye, *Nanoscale Res. Lett.*, 2009, **4**, 274.
14 J. Xu, Y. G. Zhu, H. T. Huang, Z. Xie, D. Chen and G. Z. Shen, *CrystEngComm*, 2011, **13**, 2629.
15 H. M. Sung-Suh, J. R. Choi, H. J. Hah, S. M. Koo and Y. C. Bae, *J. Photochem. Photobiol., A*, 2004, **163**, 37.
16 T. Wu, G. Liu, J. Zhao, H. Hidaka and N. Serpone, *J. Phys. Chem. B*, 1998, **102**, 5845.
17 F. Zhang, J. Zhao, L. Zang, T. Shen, H. Hidaka, E. Pelizzetti and N. Serpone, *J. Mol. Catal. A: Chem.*, 1997, **120**, 173.
18 J. M. Wu and T. W. Zhang, *J. Photochem. Photobiol., A*, 2004, **162**, 171.
19 F. Yang, Y. takahashi and N. Sakai, *J. Phys. Chem. C.*, 2011, **115**, 18270.
20 D. Chen, S. X. Ouyang and J. H. Ye, *Nanoscale Res. Lett.*, 2009, **4**, 274.
21 J. Xu, W. Meng, Y. Zhang, L. Lei and C. S. Guo, *Appl. Catal., B*, 2011, **107**, 355.
22 G. Q. Li, N. Yang, X. L. Yang, W. L. Wang and W. F. Zhang, *J. Phys. Chem. C*, 2011, **115**, 13734.
23 P. Schmitt, N. Brem, S. Schunk and C. Feldmann, *Adv. Funct. Mater.*, 2011, **21**, 3037.
24 X. C. Song, Y. F. Zheng, R. Ma, Y. Y. Zhang and H. Y. Yin, *J. Hazard. Mater.*, 2011, **192**, 186.
25 D. Chen and J. H. Ye, *J. Phys. Chem. Solids*, 2007, **68**, 2317.
26 W. M Du, J. Zhu, S. X. Li and X. F. Qian, *Cryst. Growth Des.*, 2008, **8**, 2130.
27 N. Z. Bao, L. M. Shen, T. Takata and K. Domen, *Chem. Mater.*, 2008, **20**, 110.
28 D. Chen, G. Z. Shen, K. B. Tang, S. J. Lei, H. G. Zheng and Y. T. Qian, *J. Cryst. Growth*, 2004, **260**, 469.
29 M. Muller, R. Zentel, T. Maka, S. G. Romanov and C. M. S. Torres, *Adv. Mater.*, 2000, **12**, 1499.
30 S. S. Hegde, A. G. Kunjomana, K. A. Chandrasekharan, K. Ramesh and M. Prashantha, *Phys. B*, 2011, **406**, 1143.
31 Y. Lei, S. Song, W. Fan, Y. Xing and H. Zhang, *J. Phys. Chem. C*, 2009, **113**, 1280.
32 Y. C. Zhang, Z. N. Du, K. W. Li and M. Zhang, *Sep. Purif. Technol.*, 2011, **81**, 101.
33 W. Du, D. Deng, Z. Han, W. Xiao, C. Bian and X. Qian, *Cryst. Eng. Comm*, 2011, **13**, 2071.
34 Y. C. Zhang, J. Li, M. Zhang and D. D. Dionysiou, *Environ. Sci. Technol.*, 2011, **45**, 9324.
35 S. Sohila, M. Rajalakshmi, C. Ghosh, A. K. Arora and C. Muthamizhchelvan, *J. Alloys Compd.*, 2011, **509**, 5843.
36 P. M. Nikolic, P. Lj Milikovic, B. Mihajlovic and Lavrencic, *J. Phys. C: Solid State Phys.*, 1977, **10**, L289.
37 S. Sohila, M. Rajalakshmi, C. Ghosh, A. K. Arora and C. Muthamizhchelvan, *J. Alloys Compd.*, 2011, **509**, 5843.
38 G. Lucovsky and J. C. Mikkelsen Jr, *Phys. Rev. B: Solid State*, 1976, **14**, 1663.
39 H. Fu, L. Zhang, W. Yao and Y. Zhu, *Appl. Catal., B*, 2006, **66**, 100.
40 J. Tang, Z. Zou and J. Ye, *J. Phys. Chem. B*, 2003, **107**, 14265.
41 G. Li, N. Yang, W. Wang and W. F. Zhang, *Electrochim. Acta*, 2010, **55**, 7235.
42 Y. Xu, N. Al-Salim, C. W. Bumby and R. D. Tilley, *J. Am. Chem. Soc.*, 2009, **131**, 15990.
43 S. G. Hickey, C. Waurisch, B. Rellinghaus and A. Eychmuller, *J. Am. Chem. Soc.*, 2008, **130**, 14978.
44 Z. R. Wang, H. Wang, B. Liu, W. Z. Qiu, J. Zhang, S. H. Ran, H. T. Huang, J. Xu, H. W. Han, D. Chen and G. Z. Shen, *ACS Nano*, 2011, **5**, 8412.
45 H. Ye, H. S. Park, V. A. Akhavan, B. W. Goodfellow, M. G. Panthani, B. A. Korgel and A. J. Bard, *J. Phys. Chem. C*, 2011, **115**, 234.
46 S. G. Hickey, C. Waurisch, B. Rellinghaus and A. Eychmuller, *J. Am. Chem. Soc.*, 2008, **130**, 14978.
47 Y. C. Zhang, Z. N. Du, S. Y. Li and M. Zhang, *Appl. Catal., B*, 2010, **95**, 153.
48 C. Yang, W. Wang, Z. Shan and F. Huang, *J. Solid State Chem.*, 2009, **182**, 807.
49 P. Tang, H. Chen, F. Cao, G. Pan, K. Wang, M. Xu and Y. Tong, *Mater. Lett.*, 2011, **65**, 450.
50 Y. Lei, S. Song, W. Fan, Y. Xing and H. Zhang, *J. Phys. Chem. C*, 2009, **113**, 1280.